Numerical analysis of fractional partial differential equations applied to polymeric visco-elastic Euler-Bernoulli beam under quasi-static loads

Lei Wang, Yiming Chen, Gang Cheng, Thierry Barrière

Version of Record: https://www.sciencedirect.com/science/article/pii/S0960077920306512
Manuscript_f23218633dbc4cf7b08bdd7ecb177517

Numerical analysis of fractional partial differential equations applied to polymeric visco-elastic Euler-Bernoulli beam under quasi-static loads

Lei Wang[a], Yiming Chen[a, c], Gang Cheng[b,*], Thierry Barrière[c]

[a]*College of Sciences, Yanshan University, 066004 Qinhuangdao, Hebei, China*

[b]*INSA Centre Val de Loire, Univ. Tours, Univ. Orléans, LaMé, 3 rue de la chocolaterie, BP 3410, 41034 Blois, France*

[c]*Univ. Bourgogne Franche-Comté, FEMTO-ST Institute, CNRS/ENSMM/UTBM, Department of Applied Mechanics, 25000 Besançon, France*

Abstract：

In this paper, an effective numerical algorithm based on shifted Chebyshev polynomials is proposed to solve the fractional partial differential equations applied to polymeric visco-elastic problems in the time-space domain under quasi-static loads. The governing equations using local fractional rheological models based on visco-elastic properties with fractional derivatives are established. The integer and fractional differential operator matrices of polynomials are derived according to the properties of shifted Chebyshev polynomials. The fractional order governing equation is rewritten into the form of matrix product by using the polynomial to approximate the unknown function. The collocation method is used to discretize the variables and transform the original problem into an algebraic equation system. The numerical solutions of the governing equations are obtained directly in the time-domain. In addition, an error analysis including the correction method is performed. The numerical examples have been performed to identify the sensibility of the proposed governing equations and to evaluate the efficiency and accuracy of the proposed algorithm.

Keywords： Fractional calculus, Fractional partial differential equation, Fractional rheological models, Visco-elastic properties, Euler-Bernoulli beam, Shifted Chebyshev polynomials.

1. Introduction

The polymeric material has gradually received the researchers' attentions due to its elastic and viscous behavior and high-efficiency vibration damping effect. As a vibration attenuating material, the polymer absorbs the vibration energy during mechanical vibration and converts it into heat, electric, magnetic energy to be consumed, thereby effectively reducing the structural vibration and noise. Nowadays, the polymeric material has been widely used in the fields of aerospace, construction and mechanical engineering.

Poly (ether ether ketone) (PEEK), a special engineering polymeric material, is a semi-crystalline thermoplastic polymer with excellent mechanical properties including high-temperature resistance, high-rigidity, high fracture toughness, dimensional stability and stable chemical

properties. It plays an increasingly important role in electronics, aerospace, automotive and manufacturing field. The visco-elastic effects in PEEK and its composites have been specifically studied by D'Amore et al. [1].

High-density polyethylene (HDPE) is a highly crystalline and non-polar thermoplastic polymer with high-strength to weight ratio and excellent properties such as water resistance and dielectric strength. It is widely used as the basic material in the packaging, piping and other fields. The visco-elastic behavior of HDPE has been intensively investigated in the long-term loading (tensile and compressive creep tests) by Elleuch and Taktak [2]. Lai and Bakker [3] effectuated the tensile creep tests at different stress levels from 2 to 6 MPa and physical aging from 10^0 to 10^4 s.

The long-term creep behavior was predicted by using a non-linear creep model including the physical aging effects. Guo and Bradshaw [4] studied the effect of transient creep and stress-relaxation of PEEK. Based on the HDPE and PEEK creep experimental data, Xu et al. [5] proposed finite element, fractional Maxwell, fractional Kelvin-Voight and fractional Poynting-Thomson models to describe their visco-elastic behavior.

Fractional order has better memory than integer order, which permits to describe the polymeric material's visco-elastic behavior more accurately. Gement [6] firstly established a visco-elastic constitutive model using fractional derivatives. This rheological model can be used to well describe the mechanical properties with fewer experimental parameters.

A significant amount of work was effectuated to investigate the visco-elastic properties of the polymeric materials by using constitutive rheological models containing fractional derivatives [7]. For example, Leung et al. [8] studied the non-linear steady-state vibrations of visco-elastic polymeric arches with fractional derivatives control. Lewandowski et al. [9] explored the dynamics of polymeric damper frames based on the fractional derivative rheological model. Kang et al. [10] established a fractional non-linear model to describe the creep behavior by taking into account the visco-elastic-plastic characteristics and damage effects. Gioacchino et al. [11] used a fractional-order state-variable expansion to establish a constitutive equation, and implement a numerical method to calculate the random response of a non-local fractional model under Gaussian white noise.

The visco-elastic behavior of polymeric materials and their constitutive rheological behavior modelling have gradually received the researchers' attention. A large number of fractional models have been intensively investigated to describe their visco-elastic properties. Lewandowski et al. [12] used a fractional Zener model to describe the non-linear vibration of a visco-elastic composite beam composed by the elastic and visco-elastic layers. The effect of harmonic force on non-linear vibration was investigated. Baum et al. [13] applied a four-parameter rheological model with fractional derivatives to describe the mechanical properties of the multi-layer composite beam. This innovative method was validated in order to determine the dynamic properties of the composite beam. Cortes et al. [14] used a five-parameter fractional derivative model to study the transient dynamics of a cantilever beam with different damping values under various loading conditions. Bahraini et al. [15] established the fractional four-parameter derivative model to calculate the large deflection of the visco-elastic beams and the corresponding non-linear analysis was realized by finite element method. Paola et al. [16] examined the response of fractional visco-elastic Euler-Bernoulli beam under quasi-static and dynamic loads. He et al. [17] used a fractional-order time derivative damping model to study the large-scale free and forced vibration response of the carbon nanotubes/polymer laminated multi-scale composite beams.

The numerical algorithm to solve the vibration analysis equations based on these fractional rheological models with visco-elastic properties are well documented in the literature reviews. The determination of the numerical solution of the governing equations is more intractable, due to the complexity of the fractional derivatives. Laplace or Fourier transforms have been widely used to convert the time-domain problem into frequency-domain problem. For example, Lewandowski et al. [13] used the virtual work principle and the Laplace transform to derive the frequency-domain motion equation for the dynamic analysis on the polymeric multi-layer beam. The other operational methods in fractional calculus including the finite element method, multi-scale method, Galerkin method and the variational iteration method are also found from the recent literature. Chang et al. [18] used the variable-domain finite element method to derive the motion equation to study the vibration and stability of the axial moving beam. Friswell et al. [19] used the finite element method to analyze the dynamic characteristics of polymeric beams under different boundary conditions. Demir et al. [20] established a general model in the dynamics of beams with fractional derivatives and solved the motion equation by multi-scale method. The conclusion is that the coefficient of the fractional derivative affects the stability of natural frequencies and vibration amplitudes. Permoon et al. [21] used the Galerkin method to discretize the motion equation into a set of linear ordinary differential equations and then studied the forced vibration of beams. Martinez-Agirre et al. [22] studied the harmonic response of the constrained layer damped cantilever beam and analyzed the damping structure system by using the complex modal superposition method. Based on the constitutive relation in the form of genetic integral algorithm, Martin [23] established the mathematical model for the dynamic analysis of beams with visco-elastic properties by using Galerkin and variational iteration methods for both quasi-static and dynamic analysis.

The polynomial algorithm is quite suitable for solving the fractional equation because of its rapidity, high-efficiency and high-accuracy. The polynomial approximation method, such as Legendre polynomial method [24,25], Chebyshev wavelet method [26,27], Bernoulli wavelet method [28], Bernstein polynomial method [29,30] and shifted Chebyshev polynomials (SCPs) method [31] are usually used to find the numerical solutions of the fractional equations. The SCPs method can be used to approximate the unknown function on the extended interval, which makes it easier to solve the fractional differential equations with different physical mechanisms governing and historical background. The SCPs is used as a basis to derive its integer order and fractional order differential operator matrices. The governing equations are transformed into a system of algebraic equations, which can be solved easily.

In this paper, the different fractional constitutive rheological models of the polymeric visco-elastic Euler-Bernoulli beam based on the fractional derivative element (FDE) model and the fractional derivative Kelvin-Voigt (FDKV) model have been established. These models have been implemented in the vibration governing equations of the visco-elastic beam, which are solved using specific fractional derivatives and especially SCPs approximation method. The numerical solutions are calculated directly form the governing equation in the time-space domain. The error analysis is effectuated and a correction method is proposed to obtain a high-resolution numerical solution. Euler-Bernoulli beams with different material properties for two specific thermoplastic polymers (PEEK and HDPE) have been studied as benchmark numerical examples. The numerical solutions concerning the displacement, the deformation and the stress of the beams have been obtained under quasi-static load and various boundary conditions.

This paper is structured as follows, in Section 2, some preliminaries including the basic definition of fractional differential operators, the fractional rheological constitutive equations and the properties of SCPs are described. In Section 3, FDE and FDKV models have been used to establish the governing equation for different polymeric beam under different load and boundary conditions. In Section 4, the SCPs solving algorithm is described. An error analysis with the correction method is performed in Section 5. In Section 6, the numerical results of the displacement, the deformation and the stress of the Euler-Bernoulli beams are obtained and discussed to show the advantage of the proposed approach. The research work is concluded in Section 7.

2. Preliminaries and notations

2.1 The basic definition of fractional differential operator

Definition1. The Riemann-Liouville fractional differential operator $\left({}^{RL}D^{\alpha}f\right)$ of order α is defined by [32]:

$$\left({}^{RL}D^{\alpha}f\right)(y)=\begin{cases}\frac{1}{\Gamma(m-\alpha)}\frac{d^m}{dy^m}\int_0^y\frac{f(s)}{(y-s)^{\alpha-m+1}}ds,\ \alpha>0,\ m-1\le\alpha<m,\\ \frac{d^mf(y)}{dy^m},\ \alpha=m.\end{cases}\tag{1}$$

where $m\in N$, $f(y)$ is continuous over interval $(0,+\infty)$ and is integrable over any subinterval $[0,+\infty)$, α is fractional derivative order, $y>0$, α and y are real.

The gamma function, denoted by $\Gamma(.)$ is defined as $\Gamma(z)=\int_0^{\infty}e^{-y}y^{z-1}dy$ for complex arguments with positive real part.

Definition2. The Caputo definition of fractional differential operator $\left({}^{C}D^{\alpha}f\right)$ of order α is given by [33]:

$$\left({}^{C}D^{\alpha}f\right)(y)=\begin{cases}\frac{1}{\Gamma(m-\alpha)}\int_0^y\frac{f^{(m)}(\tau)}{(y-\tau)^{\alpha-m+1}}d\tau,\alpha>0,m-1\le\alpha<m,\\ \frac{d^mf(y)}{dy^m},\alpha=m.\end{cases}\tag{2}$$

The Caputo fractional derivative of distributed order is defined as:

$${}^{C}D^{\alpha}y^{\chi}=\begin{cases}0,for\ \chi\in N_0\ and\ \chi<\lceil\alpha\rceil,\\ \frac{\Gamma(\chi+1)}{\Gamma(\chi+1-\alpha)}y^{\chi-\alpha},for\ \chi\in N_0\ and\ \chi\ge\lceil\alpha\rceil\ or\ \chi\notin N_0\ and\ \chi>\lfloor\alpha\rfloor.\end{cases}\tag{3}$$

2.2 Properties of the SCPs

SCPs are considered as useful tools to solve the fractional equation in the physical problems. The well-known Chebyshev polynomials satisfy the following three-term recurrence relation:

$$F_{i+1}(c)=2cF_i(c)-F_{i-1}(c),\ i=1,2,\cdots\tag{4}$$

where $F_0(c)=1$ and $F_1(c)=c$. c is defined on the interval $[-1,1]$ and $i=1,2,\cdots$

On the interval $m\in[0,H]$, where H is a non-negative real number, the SCPs are defined by the change of variable $c=\frac{2m}{H}-1$. Let the SCPs $F_i\left(\frac{2m}{H}-1\right)$ denote by $G_i(m)$, which can be obtained as follows:

$$G_{i+1}(m)=2\left(\frac{2m}{H}-1\right)G_i(m)-G_{i-1}(m),\ i=1,2,\cdots\tag{5}$$

where $G_0(m)=1$, $G_1(m)=\frac{2m}{H}-1$.

The analytic form of $G_i(m)$ of i-degree is given by:

$$G_i(m)=i\sum_{k=0}^{i}(-1)^{i-k}\frac{(i+k-1)!2^{2k}}{(i-k)!(2k)!H^k}m^k,\ i=1,2,\cdots\tag{6}$$

where $G_i(0) = (-1)^i$ and $G_i(H) = 1$.

The orthogonally condition is

$$\int_0^H G_j(m)\, G_k(m) W_H(m) dm = h_k \tag{7}$$

where $W_H(m) = \frac{1}{\sqrt{Hm-m^2}}$ and $h_k = \begin{cases} \frac{b_k}{2}\pi, k = j, \\ 0, k \neq j, \end{cases}$ $b_0 = 2,\ b_k = 1,\ k \geq 1.$

The operational matrix is defined by: $\Phi_n(m) = [G_0(m), G_1(m), \dots, G_n(m)]^T$

The following equation can be obtained:

$$\Phi_n(m) = A_n Z_n(m) \tag{8}$$

where $Z_n(m) = [1, m, \dots, m^n]^T$, and A_n is the SCPs coefficient matrix given as follows:

$$A_n = \begin{bmatrix} P_{0,0} & 0 & \cdots & 0 \\ P_{1,0} & P_{1,1} & \cdots & 0 \\ \vdots & \vdots & \ddots & \vdots \\ P_{n,0} & P_{n,1} & \cdots & P_{n,n} \end{bmatrix} \tag{9}$$

where $\begin{cases} P_{0,0} = 1, \\ P_{i,j} = 2\left(\frac{2}{H} P_{i-1,j-1} - P_{i-1,j}\right) - P_{i-2,j}, \\ P_{i,j} = 0, for\ i < j\ or\ i < 0\ or\ j < 0. \end{cases}$

Obviously, A_n is full rank and reversible.

2.3 Definition of the visco-elastic constitutive relations based on fractional derivative models

The general form of a one-dimensional generalized fractional constitutive equation describing the stress-strain relationship of a visco-elastic material is [34]:

$$\sum_{\kappa=0}^{n} \mu_\kappa \frac{d^{p_\kappa}\sigma}{dt^{p_\kappa}} = \sum_{\kappa=0}^{n} \eta_\kappa \frac{d^{q_\kappa}\varepsilon}{dt^{q_\kappa}} \tag{10}$$

where d^κ/dt^κ uses the Caputo type fractional differential definition, t is the time, σ is the stress, ε is the strain, and μ_κ, η_κ are the material constants. κ is a positive integer. p_κ, q_κ are real numbers corresponding to fractional order of the time derivative.

Du et al. [35] proved that the physical meaning of fractional order is an indicator of memory, which is suitable to describe the memory phenomena in different disciplines. It is more accurately to describe the visco-elastic behavior of the polymeric material by using the fractional derivative constitutive equations.

When $p_\kappa, q_\kappa = 0$, the constitutive equation becomes ideal elastic behavior law or Hooke's law. When $p_\kappa = 0, q_\kappa = 1$, the constitutive equation becomes ideal viscous behavior law or Newton's law. When $0 < q_\kappa < 1$, the constitutive equation could be used to describe the physical behavior of a viscoelastic material.

In the current visco-elastic constitutive fractional derivative models, the first order derivatives d/dt are replaced by the fractional derivatives $d^{q_\kappa}/dt^{q_\kappa}$ with $0 < q_\kappa < 1$.

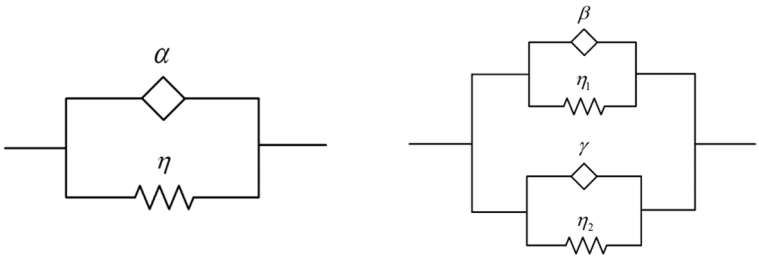

(a) (b)

FIGURE 1 Schematic representation of visco-elastic model: (a) FDE model and (b) FDKV model.

The simplest visco-elastic fractional derivative model is the FDE model [5] as shown in **Fig. 1(a)**. The stress-strain relationship could be presented by the following equation:

$$\sigma = \eta \frac{d^{\alpha}\varepsilon}{dt^{\alpha}} \tag{11}$$

where η, α represent the material constants, α is a real number within $(0, 1)$. Here, $\frac{d^{\alpha}}{dt^{\alpha}}$ is the Riemann-Liouville fractional differential operator of order α.

The two-dimensional FDE model can be expressed as:

$$\sigma(x,t) = \eta\, {}^{C}D^{\alpha}\varepsilon(x,t) \tag{12}$$

where x is the position and ${}^{C}D^{\alpha}$ is Caputo fractional differential operator, defined in Eq. (2).

When two fractional derivative elements are arranged in parallel, as shown in **Fig. 1(b)**, it is the FDKV model[5], in which the constitutive equation is defined as follows:

$$\sigma = \eta_1 \frac{d^{\beta}\varepsilon}{dt^{\beta}} + \eta_2 \frac{d^{\gamma}\varepsilon}{dt^{\gamma}} \tag{13}$$

where $\eta_1, \eta_2, \beta, \gamma$ are the material constants, and β, γ are the real number within $(0, 1)$.

The two-dimensional FDKV model can be expressed as:

$$\sigma(x,t) = \eta_1\, {}^{C}D^{\beta}\varepsilon(x,t) + \eta_2\, {}^{C}D^{\gamma}\varepsilon(x,t) \tag{14}$$

where ${}^{C}D^{\beta}$, ${}^{C}D^{\gamma}$ is Caputo fractional differential operator.

3. The governing equations of the visco-elastic Euler-Bernoulli beam

3.1 Beam governing equation with the FDKV model

A visco-elastic Euler-Bernoulli beam, fixed at both ends, is considered in this study. A distributed load is applied on the vertical direction of the beam. The beam is treated as a visco-elastic material. The bending deformation occurs on the beam in the vertical direction, as shown in **Fig. 2**, in which $\omega(x,t)$ is the beam deflection, $f(x,t)$ is the distributed load, l is the length of the beam, b is the width of a rectangular cross section and h is the height of a rectangular cross section.

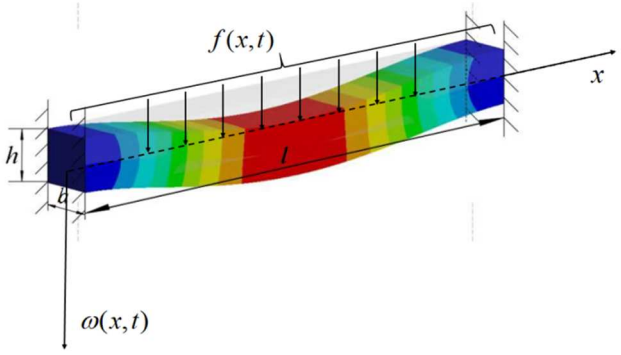

FIGURE 2 The bending deformation of the visco-elastic Euler-Bernoulli beam under the distributed load.

Based on **Fig. 2**, the most important displacement of the beam is the deflection. The beam deflection varies in function of x and t. The differential equation of the transverse oscillation has been studied by Martin [36] and the integral differential equation of the beam is given by:

$$\rho A \frac{\partial^2 \omega(x,t)}{\partial t^2} + \frac{\partial^2 M(x,t)}{\partial x^2} = f(x,t) \tag{15}$$

where ρ is the density of the material and A is the square cross-sectional area. The bending moment $M(x,t)$ of the beam is written as:

$$M(x,t) = \int_A z\,\sigma(x,t)dA \tag{16}$$

where $\sigma(x,t)$ is the normal stress on the cross-section and z represent the transverse coordinate.

Based on the Euler-Bernoulli beam theory, the relation between strain and displacement can be expressed as:

$$\varepsilon(x,t) = z\frac{\partial^2 \omega(x,t)}{\partial x^2} \tag{17}$$

When the FDKV model is used to describe the visco-elastic behavior of the beam, the stress of the beam can be obtained by using Eqs. (14) and (17):

$$\sigma(x,t) = \eta_1\, {}^C D^{\beta} z\frac{\partial^2 \omega(x,t)}{\partial x^2} + \eta_2\, {}^C D^{\gamma} z\frac{\partial^2 \omega(x,t)}{\partial x^2} \tag{18}$$

Based on Eqs (16) and (18), the beam bending moment $M(x,t)$ is equal to:

$$M(x,t) = \eta_1 I\, {}^C D^{\beta} \frac{\partial^2 \omega(x,t)}{\partial x^2} + \eta_2 I\, {}^C D^{\gamma} \frac{\partial^2 \omega(x,t)}{\partial x^2} \tag{19}$$

where the moment inertia is $I = \int_A z^2\, dA = \frac{bh^3}{12}$.

Based on Eqs. (15) and (19), the bending vibration equation of the visco-elastic Euler-Bernoulli beam with FDKV model is obtained:

$$\rho A \frac{\partial^2 \omega(x,t)}{\partial t^2} + \eta_1 I\, {}^C D^{\beta} \frac{\partial^4 \omega(x,t)}{\partial x^4} + \eta_2 I\, {}^C D^{\gamma} \frac{\partial^4 \omega(x,t)}{\partial x^4} = f(x,t) \tag{20}$$

3.2 Beam governing equation under the FDE model

When the FDE model is used to describe the visco-elastic behavior of the beam, the stress of the beam is proposed:

$$\sigma(x,t) = \eta\, {}^{C}D^{\alpha} z \frac{\partial^2 \omega(x,t)}{\partial x^2} \tag{21}$$

where $\alpha \in (0,1)$.

Based on Eqs. (16) and (21), the beam bending moment $M(x,t)$ can be rewritten as:

$$M(x,t) = \eta I\, {}^{C}D^{\alpha} \frac{\partial^2 \omega(x,t)}{\partial x^2} \tag{22}$$

The bending vibration equation of the visco-elastic Euler-Bernoulli beam with FDE model is obtained as follows:

$$\rho A \frac{\partial^2 \omega(x,t)}{\partial t^2} + \eta I\, {}^{C}D^{\alpha} \frac{\partial^4 \omega(x,t)}{\partial x^4} = f(x,t) \tag{23}$$

4. Numerical algorithm

The approximation function based on the families of SCPs of x and t was applied to replace the real displacement function. The collocation method was used to discretize the variables x and t to transform the fractional beam governing equations into a set of algebraic equations. An error analysis was preformed to estimate the calculation accuracy.

The most important contribution of this numerical algorithm is that the numerical solution of the beam governing equation is successfully obtained with high accuracy and the obtained displacement and stress of beam is directly in time domain. The numerical algorithm is summarized in **Fig. 3**:

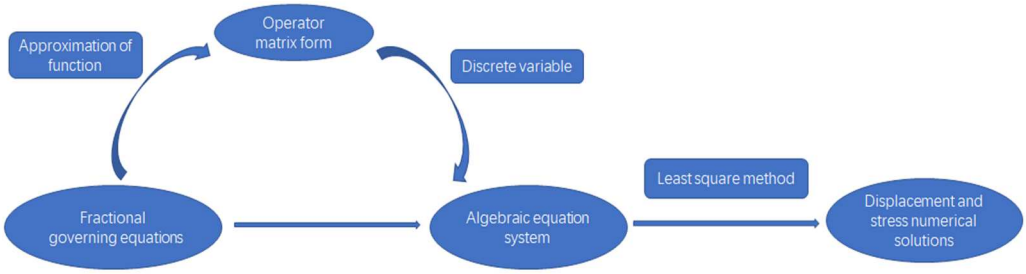

FIGURE 3 A schematic illustration of the proposed numerical algorithm.

4.1 Approximation of the beam deflection function

The beam deflection function $\omega(x,t) \in L^2([0,H] \times [0,T])$ can be expanded as the following formula:

$$\omega(x,t) = \sum_{i=0}^{\infty} \sum_{j=0}^{\infty} \omega_{ij} G_i(x) G_j(t) \tag{24}$$

where $\omega_{ij} = \frac{1}{h_i h_j} \int_0^H \int_0^T \omega(x,t) G_i(x) G_j(t) \omega_H(x) \omega_T(t) dx dt,\ i,j = 0,1,2,\cdots.$

If the truncated series are considered in Eq. (24), then it can be rewritten as:

$$\omega(x,t) \approx \sum_{i=0}^{n} \sum_{j=0}^{n} \omega_{ij} G_i(x) G_j(t) = \Phi_n^T(x) U \Phi_n(t) \tag{25}$$

where $\Phi_n(x) = [G_0(x), G_1(x), \ldots, G_n(x)]^T$, $\Phi_n(t) = [G_0(t),\ G_1(t),\ \ldots,\ G_n(t)]^T$, $U = \{u_{ij}\}_{i,j=0}^{n,n}$.

4.2 SCPs differential operator matrix of displacement function

4.2.1 First order differential operator matrix of SCPs

The first order derivative of $\Phi_n(x)$ for x can be expressed as follows by using Eq. (8):

$$\frac{d}{dx}\Phi_n(x) = \left(A_X Z_n(x)\right)' = A_X Z_n'(x) = A_X \begin{bmatrix} 1' \\ x' \\ \vdots \\ (x^n)' \end{bmatrix} = A_X \begin{bmatrix} 0 \\ 1 \\ \vdots \\ nx^{n-1} \end{bmatrix} = A_X V_{(n+1)\times(n+1)} Z_n(x) \quad (26)$$

where A_X is obtained by replacing n by X in Eq. (9), and $V_{(n+1)\times(n+1)} = \begin{bmatrix} 0 & 0 & 0 & \cdots & 0 & 0 \\ 1 & 0 & 0 & \cdots & 0 & 0 \\ 0 & 2 & 0 & \cdots & 0 & 0 \\ \vdots & \vdots & \vdots & \ddots & \vdots & \vdots \\ 0 & 0 & 0 & \cdots & 0 & 0 \\ 0 & 0 & 0 & \cdots & n & 0 \end{bmatrix}$

$Z_n(x)$ is obtained by using Eq. (8):

$$Z_n(x) = A_X^{-1}\Phi_n(x) \quad (27)$$

Based on Eqs. (26) and (27), the first order derivative of $\Phi_n(x)$ for x can be rewritten as:

$$\frac{d}{dx}\Phi_n(x) = A_X V_{(n+1)\times(n+1)} A_X^{-1}\Phi_n(x) = P_x^1 \Phi_n(x) \quad (28)$$

where $P_x^1 = A_X V_{(n+1)\times(n+1)} A_X^{-1}$ is called the first order differential operator matrix of the SCPs for x.

Based on Eqs. (25) and (28), the following equations could be obtained:

$$\frac{\partial\omega(x,t)}{\partial x} \approx \frac{\partial\left(\Phi_n^T(x) U \Phi_n(t)\right)}{\partial x} = \Phi_n^T(x)(P_x^1)^T U \Phi_n(t) = \Phi_n^T(x)\left(A_X V_{(n+1)\times(n+1)} A_X^{-1}\right)^T U \Phi_n(t) \quad (29)$$

$$\frac{\partial^4\omega(x,t)}{\partial x^4} \approx \frac{\partial^4\left(\Phi_n^T(x) U \Phi_n(t)\right)}{\partial x^4} = \Phi_n^T(x)((P_x^1)^T)^4 U \Phi_n(t) =$$

$$\Phi_n^T(x)\left(\left(A_X V_{(n+1)\times(n+1)} A_X^{-1}\right)^T\right)^4 U \Phi_n(t) \quad (30)$$

$$\frac{\partial^2\omega(x,t)}{\partial t^2} \approx \frac{\partial^2\left(\Phi_n^T(x) U \Phi_n(t)\right)}{\partial t^2} = \Phi_n^T(x) U (P_t^1)^2 \Phi_n(t) = \Phi_n^T(x) U \left(A_T V_{(n+1)\times(n+1)} A_T^{-1}\right)^2 \Phi_n(t) \quad (31)$$

where A_T is obtained by replacing n by T in Eq. (9), and $P_t^1 = A_T V_{(n+1)\times(n+1)} A_T^{-1}$ is the first order differential operator matrix of the SCPs for t.

4.2.2 Fractional order differential operator matrix of the SCPs

The fractional derivative of $\Phi_n(t)$ for t could be calculated by the following equation according to Eq. (25):

$${}^C D^\alpha \Phi_n(t) = {}^C D^\alpha\left(A_T Z_n(t)\right) = A_T\, {}^C D^\alpha Z_n(t) = A_T \begin{bmatrix} 0 \\ \frac{\Gamma(2)}{\Gamma(2-\alpha)} t^{1-\alpha} \\ \vdots \\ \frac{\Gamma(n+1)}{\Gamma(n+1-\alpha)} t^{n-\alpha} \end{bmatrix} =$$

$$A_T V_{(n+1)\times(n+1)}^{\alpha} A_T^{-1}\Phi_n(t) = P_t^\alpha \Phi_n(t) \quad (32)$$

where $P_t^\alpha = A_T V_{(n+1)\times(n+1)}^{\alpha} A_T^{-1}$ is called the fractional order differential operator matrix of the SCPs for t and

$$\mathrm{V}_{(n+1)\times(n+1)}^{\alpha} = \begin{bmatrix} 0 & 0 & \cdots & 0 \\ 0 & \frac{\Gamma(2)}{\Gamma(2-\alpha)}\mathrm{t}^{-\alpha} & \cdots & 0 \\ \vdots & \vdots & \ddots & \vdots \\ 0 & 0 & \cdots & \frac{\Gamma(n+1)}{\Gamma(n+1-\alpha)}\mathrm{t}^{-\alpha} \end{bmatrix} \quad (33)$$

Based on Eq. (32), the following equations could be found:

$$ {}_C D^{\beta} \frac{\partial^4 \omega(x,t)}{\partial x^4} \approx {}_C D^{\beta} \Phi_n^T(x) \left(\left(A_X V_{(n+1)\times(n+1)} A_X^{-1} \right)^T \right)^4 U \Phi_n(t) = $$

$$ \Phi_n^T(x) \left(\left(A_X V_{(n+1)\times(n+1)} A_X^{-1} \right)^T \right)^4 U \, {}_C D^{\beta} \Phi_n(t) = $$

$$ \Phi_n^T(x) \left(\left(A_X V_{(n+1)\times(n+1)} A_X^{-1} \right)^T \right)^4 U A_T V_{(n+1)\times(n+1)}^{\beta} A_T^{-1} \Phi_n(t) \quad (34) $$

where $V_{(n+1)\times(n+1)}^{\beta}$ is obtained by replacing α by β in Eq. (33)

Similarly,

$$ {}_C D^{\gamma} \frac{\partial^4 \omega(x,t)}{\partial x^4} \approx {}_C D^{\gamma} \Phi_n^T(x) \left(\left(A_X V_{(n+1)\times(n+1)} A_X^{-1} \right)^T \right)^4 U \Phi_n(t) = $$

$$ \Phi_n^T(x) \left(\left(A_X V_{(n+1)\times(n+1)} A_X^{-1} \right)^T \right)^4 U \, {}_C D^{\gamma} \Phi_n(t) = $$

$$ \Phi_n^T(x) \left(\left(A_X V_{(n+1)\times(n+1)} A_X^{-1} \right)^T \right)^4 U A_T V_{(n+1)\times(n+1)}^{\gamma} A_T^{-1} \Phi_n(t) \quad (35) $$

where $V_{(n+1)\times(n+1)}^{\gamma}$ is obtained by replacing α by γ in Eq. (33).

The bending vibration equation of the visco-elastic Euler-Bernoulli beam with FDKV model, Eq. (20), could be transformed into the following form:

$$ \rho A \Phi_n^T(x) U \left(A_T V_{(n+1)\times(n+1)} A_T^{-1} \right)^2 \Phi_n(t) + \eta_1 I \Phi_n^T(x) \left(\left(A_X V_{(n+1)\times(n+1)} A_X^{-1} \right)^T \right)^4 U A_T V_{(n+1)\times(n+1)}^{\beta} $$

$$ \times A_T^{-1} \Phi_n(t) + \eta_2 I \Phi_n^T(x) \left(\left(A_X V_{(n+1)\times(n+1)} A_X^{-1} \right)^T \right)^4 U A_T V_{(n+1)\times(n+1)}^{\gamma} A_T^{-1} \Phi_n(t) = f(x,t) \quad (36) $$

Similarly, the bending vibration equation of the visco-elastic Euler-Bernoulli beam with FDE model, Eq. (23), could be transformed into the following form:

$$ \rho A \Phi_n^T(x) U \left(A_T V_{(n+1)\times(n+1)} A_T^{-1} \right)^2 \Phi_n(t) + \eta I \Phi_n^T(x) \left(\left(A_X V_{(n+1)\times(n+1)} A_X^{-1} \right)^T \right)^4 U A_T V_{(n+1)\times(n+1)}^{\alpha} $$

$$ \times A_T^{-1} \Phi_n(t) = f(x,t) \quad (37) $$

Based on the collocation method, the reasonable match points $x_i = \frac{2i-1}{2(n+1)} H$, $i = 0, 1, 2, \cdots, n$, $t_j = \frac{2j-1}{2(n+1)} T$, $j = 0, 1, 2, \cdots, n$. have been used to discretize the variable (x, t) to $\left(x_i, t_j\right)$. Eqs. (36) and (37) are transformed into a set of algebraic equations. The coefficient ω_{ij}($i = 0, 1, 2, \cdots, n$; $j = 0, 1, 2, \cdots, n$) is determinate by using Matlab platform and least square method. The numerical solution of the fractional derivative equations can be obtained.

5. Error Analysis

5.1 Error correction

The equation to be solved is defined as the operator $L[*]$:

$$ L[\omega(x,t)] = 0 \quad (38) $$

where $\omega(x,t)$ is the exact solution of the beam deflection.

The numerical solution of the beam deflection is $\omega_n(x,t)$. If $\omega_n(x,t)$ is brought into Eq. (38) there must be a residual term called the residual function $R_n(x,t)$:

$$ L[\omega_n(x,t)] = R_n(x,t) \quad (39) $$

So:

$$ L[\omega(x,t)] - L[\omega_n(x,t)] = -R_n(x,t) \quad (40) $$

then, $\omega_n(x,t)$ can be expressed as:

$$L[\omega_n(x,t)] = \frac{\partial^2 \omega_n(x,t)}{\partial t^2} + {}^{C}D^{\beta}\frac{\partial^4 \omega_n(x,t)}{\partial x^4} + {}^{C}D^{\gamma}\frac{\partial^4 \omega_n(x,t)}{\partial x^4} - f(x,t) = R_n(x,t) \tag{41}$$

The absolute error function is defined as $e_n(x,t)$, which satisfies:

$$e_n(x,t) = \omega(x,t) - \omega_n(x,t) \tag{42}$$

Based on the definition of $L[*]$:

$$L[e_n(x,t)] = L[\omega(x,t)] - L[\omega_n(x,t)] = -R_n(x,t) \tag{43}$$

Hence, Eq. (43) is rewritten as:

$$L[e_n(x,t)] = \frac{\partial^2 e_n(x,t)}{\partial t^2} + {}^{C}D^{\beta}\frac{\partial^4 e_n(x,t)}{\partial x^4} + {}^{C}D^{\gamma}\frac{\partial^4 e_n(x,t)}{\partial x^4} - f(x,t) = -R_n(x,t) \tag{44}$$

where $e_n(x,t)$ can be approximated by $e^*(x,t)$, which is calculated by using the algorithm proposed in the previous section. $L[e_n(x,t)]$ is the approximate error function in Eq. (44).

Therefore, the corrected solution $\omega^*(x,t)$ can be obtained as follows:

$$\omega^*(x,t) = \omega_n(x,t) + e^*(x,t) \tag{45}$$

Furthermore, correction error function $E(x,t)$ can be expressed as:

$$E(x,t) = e_n(x,t) - e^*(x,t) = \omega(x,t) - \omega_n(x,t) - e^*(x,t) \tag{46}$$

5.2 Absolute error bound of correction solution method

Theorem1. Let $\omega(x,t)$ and $\omega^*(x,t)$ are the exact and correction solutions of the governing equations Eq. (20). If the continuous function $\omega(x,t)$ has K order partial derivative on the interval $\Lambda \in [0,X] \times [0,T]$, where $K = 0, 1, \cdots, M$, then:

$$|\omega(x,t) - \omega^*(x,t)| \le |R_M| + \left|\omega_{T,M}(x,t) - \omega^*(x,t)\right| \tag{47}$$

where $\omega_{T,M}(x,t)$ is M^{th} order Taylor series expansion of $\omega(x,t)$ in the neighborhood of (x_0,t_0), and R_M represents the remainder of the Taylor series expansion.

Proof: If the function $\omega(x,t)$ is continuous in a neighborhood around (x_0,t_0), and (x_0+h, t_0+k) is any point in the neighborhood. Since $\omega(x,t)$ has an $M+1$ order differential, $\omega(x,t)$ can be expressed as a Taylor series expansion:

$$\omega(x,t) = \sum_{n=0}^{M}\left(h\frac{\partial}{\partial x} + k\frac{\partial}{\partial t}\right)^{(n)}\omega(x_0,t_0) + R_M \tag{48}$$

where R_M is the remainder of the Taylor series expansion:

$$R_M = \frac{1}{(M+1)!}\left(h\frac{\partial}{\partial x} + k\frac{\partial}{\partial t}\right)^{M+1}\omega(x_0+\theta h, t_0+\theta k),\ 0 < \theta < 1 \tag{49}$$

Furthermore, the M^{th} Taylor series expansion $\omega_{T,M}(x,t)$ of $\omega(x,t)$ in the neighborhood of (x_0,t_0) is obtained:

$$\omega(x,t) - \omega_{T,M}(x,t) = R_M \tag{50}$$

Based on Eq. (50) and the triangle inequality, the absolute error bound of the corrected solution could be obtained:

$$|\omega(x,t) - \omega^*(x,t)| = \left|\omega(x,t) - \omega^*(x,t) + \omega_{T,M}(x,t) - \omega_{T,M}(x,t)\right| \le \left|\omega(x,t) - \omega_{T,M}(x,t)\right| + \left|\omega_{T,M}(x,t) - \omega^*(x,t)\right| = |R_M| + \left|\omega_{T,M}(x,t) - \omega^*(x,t)\right| \tag{51}$$

6. Numerical analysis

6.1 Mathematical example

A general mathematical example is proposed, associated with its exact solution. The general mathematical example is solved by the proposed SCPs numerical algorithm. The numerical solution is compared with the exact solution to verify the accuracy and efficiency of the proposed algorithm. The general mathematical example is similar with the governing equation with FDE model, therefore the parameters in the example are arbitrary values and have no physical meanings. The general mathematical example is given by:

$$50\frac{\partial^2\omega(x,t)}{\partial t^2} + {}^{C}D^{\alpha}\frac{\partial^4\omega(x,t)}{\partial x^4} = f(x,t) \tag{52}$$

where $\alpha = 0.5$, $f(x,t) = 100x^2(2-x)^2 + 24\frac{\Gamma(3)}{\Gamma(2.5)}t^{1.5}$.

The boundary and initial conditions are:

$$\begin{cases} \omega(0,t) = \omega(2,t) = 0 \\ \omega'(0,t) = \omega'(2,t) = 0 \\ \omega(x,0) = \omega'(x,0) = 0 \end{cases} \tag{53}$$

The exact solution of the Eq. (52) is $\omega(x,t) = x^2(2-x)^2t^2$.

Based on the SCPs algorithm in Section 4, the equation (52) is transformed into the following matrix form:

$$50\Phi_n^T(x)U\left(A_TV_{(n+1)\times(n+1)}A_T^{-1}\right)^2\Phi_n(t) + \Phi_n^T(x)\left(\left(A_XV_{(n+1)\times(n+1)}A_X^{-1}\right)^T\right)^4 UA_TV^{\alpha}_{(n+1)\times(n+1)}$$

$$\times A_T^{-1}\Phi_n(t) = f(x,t) \tag{54}$$

By using the collocation method, the variables are discretized, and then the matrix form of the square is transformed into algebraic equations. Through the MATLAB software and the least square method, the coefficient matrix U can be obtained as follows:

$$U=\begin{bmatrix} u_{11} & u_{12} & u_{13} & u_{14} & u_{15} \\ u_{21} & u_{22} & u_{23} & u_{24} & u_{25} \\ u_{31} & u_{32} & u_{33} & u_{34} & u_{35} \\ u_{41} & u_{42} & u_{43} & u_{44} & u_{45} \\ u_{51} & u_{52} & u_{53} & u_{54} & u_{55} \end{bmatrix} \tag{55}$$

where $u_{11} = 0.140625000000007$, $u_{12} = 0.187500000000017$, $u_{13} = 0.0468750000000064$, $u_{14} = -4.02766416350686\text{e}-16$, $u_{15} = 2.36054784644246\text{e}-16$,

$u_{21} = 2.45752190233397\text{e}-16$, $u_{22} = -1.27968731819555\text{e}-15$, $u_{23} = -2.93215171889535\text{e}-16$, $u_{24} = -1.13086243822289\text{e}-16$,

$u_{25} = -9.57933713723775\text{e}-17$, $u_{31} = -0.187500000000003$,

$u_{32} = -0.250000000000000$, $u_{33} = -0.0624999999999987$, $u_{34} = -1.18053054442575\text{e}-15$, $u_{35} = 4.83433281445094\text{e}-16$,

$u_{41} = -7.81117159281965\text{e}-16$, $u_{42} = -2.59342907822039\text{e}-15$, $u_{43} = -2.03364034427167\text{e}-16$, $u_{44} = 9.82413826167261\text{e}-17$,

$u_{45} = -1.66240142066007\text{e}-18$, $u_{51} = 0.0468750000000009$,

$u_{52} = 0.0468750000000009$, $u_{53} = 0.0156250000000014$,

$u_{54} = -1.09690902988797\text{e}-15$, $u_{55} = 2.88041818902505\text{e}-16$.

The preceding proposed method, was applied to find the solution of Eq. (52). The SCPs numerical algorithm with the number of terms equal to 4 ($n = 4$) was used to calculate the

numerical solution $\omega_n(x,t)$ of Eq. (52). The comparison between its numerical solution and its exact solution for different t and x are shown in **Fig. 4**. The numerical results seem to be consistent with the exact solutions, which proves a high accuracy of the proposed algorithm in the approximation of the numerical solution of the fractional derivative equations.

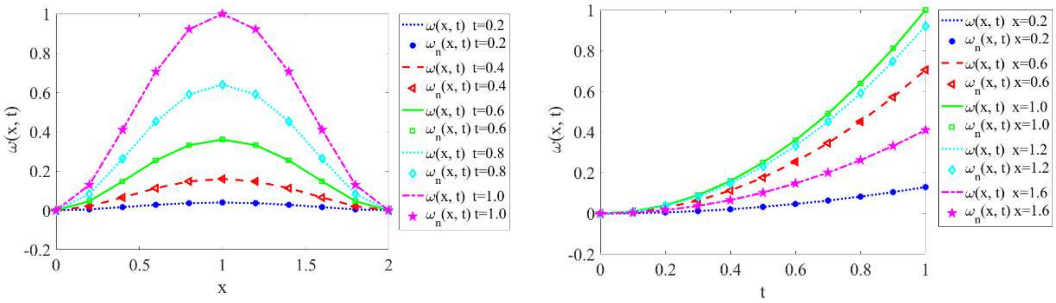

(a) (b)

FIGURE 4 Comparison of exact and numerical solutions of $\omega(x,t)$ in the equation for different values: (a) t; (b) x.

The absolute error function, defined in Eq. (42), is used to calculate the difference between the numerical and exact solutions. The absolute error at different t: $t = 0$, $t = 0.2$, $t = 0.4$, $t = 0.6$, $t = 0.8$, $t = 1$ are shown in **Fig. 5**. The absolute errors are around 10^{-14}, which confirm that a high-precision has been achieved by using the proposed algorithm. The algorithm can effectively solve the fractional partial differential equations.

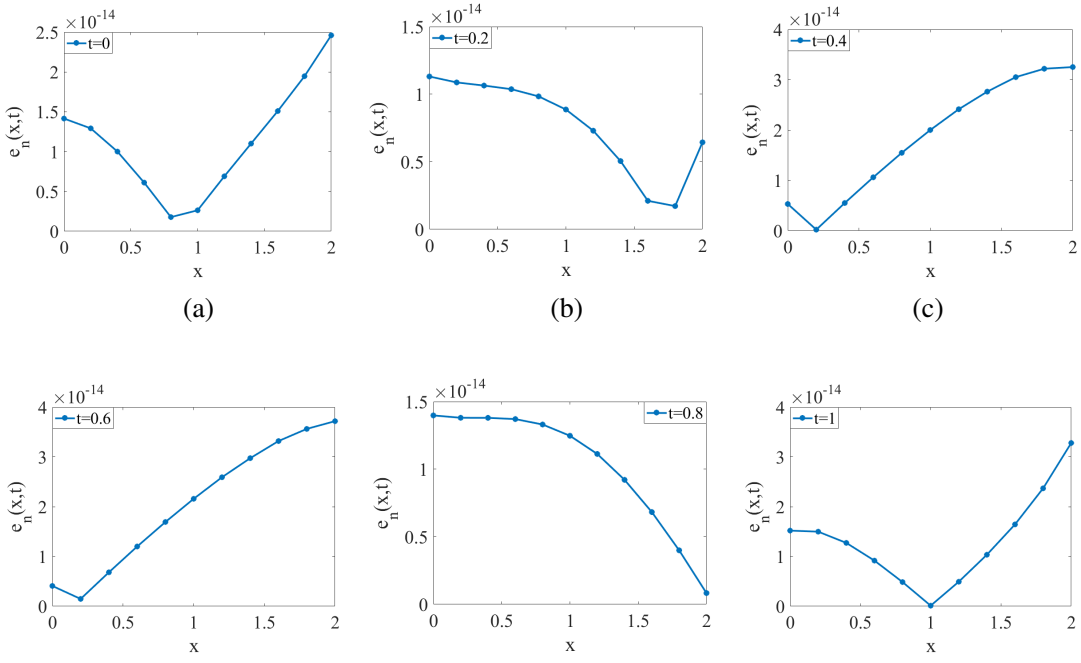

(a) (b) (c)

(d) (e) (f)

FIGURE 5 The evolution of absolute error between the numerical solution of the equation when t takes different values: (a) $t = 0$; (b) $t = 0.2$; (c) $t = 0.4$; (d) $t = 0.6$; (e) $t = 0.8$; (f) $t = 1$.

Since the relative error can better explain the validity of the method, the relative error $\hat{e}(x,t)$ of the equation is introduced when solving the example equation. The relative error $\hat{e}(x,t)$ can be expressed as:

$$\hat{e}(x,t) = \left|\frac{\omega_n(x,t)-\omega(x,t)}{\omega(x,t)}\right| \tag{56}$$

The number of terms of the SCPs may affect the calculate accuracy during the approximation of the exact solution of the fractional partial differential equations. Different number of terms of the SCPs $n = 4$, $n = 5$, $n = 6$ has been proposed to solve the fractional equations to investigate its influence on the numerical calculation efficiency. The absolute and relative errors of the numerical and exact solutions at same (x,t) with the terms of the SCPs equal to 4, 5 and 6 are summarized in **Table 1**. It shows that a high-precision of numerical calculation is obtained even with a small number of terms of SCPs. The absolute error between the numerical and the exact solutions decreases when the number of terms of the SCPs increases. When $n = 6$, the absolute error can reach 10^{-17}. The concept of relative error is introduced to describe the precision between the numerical and the exact solutions, the accuracy performance of the algorithm is shown in this numerical example.

TABLE 1 Absolute and relative errors of the equation with different values of n.

t	x	$n=4$		$n=5$		$n=6$	
		absolute error	relative error	absolute error	relative error	absolute error	relative error
0.2	0.4	2.44×10^{-15}	1.49×10^{-13}	4.68×10^{-16}	2.86×10^{-14}	3.12×10^{-17}	1.91×10^{-15}
	1.0	5.93×10^{-15}	1.48×10^{-13}	3.05×10^{-15}	7.63×10^{-14}	1.58×10^{-15}	3.96×10^{-14}
	1.6	3.89×10^{-15}	2.37×10^{-13}	3.28×10^{-15}	2.00×10^{-13}	1.89×10^{-15}	1.15×10^{-13}
0.6	0.4	2.46×10^{-15}	1.67×10^{-14}	1.88×10^{-15}	1.28×10^{-14}	1.76×10^{-15}	1.19×10^{-14}
	1.0	1.95×10^{-14}	5.43×10^{-14}	2.22×10^{-15}	6.17×10^{-15}	2.11×10^{-15}	5.86×10^{-15}
	1.6	3.71×10^{-14}	2.51×10^{-13}	1.33×10^{-15}	9.03×10^{-15}	8.88×10^{-16}	6.02×10^{-15}
1.0	0.4	1.44×10^{-14}	3.53×10^{-14}	1.23×10^{-16}	2.99×10^{-16}	7.47×10^{-16}	1.82×10^{-15}
	1.0	5.08×10^{-15}	5.08×10^{-15}	1.78×10^{-15}	1.78×10^{-15}	5.21×10^{-16}	5.21×10^{-16}
	1.6	1.08×10^{-14}	2.63×10^{-14}	1.66×10^{-15}	4.06×10^{-15}	1.64×10^{-15}	4.00×10^{-15}

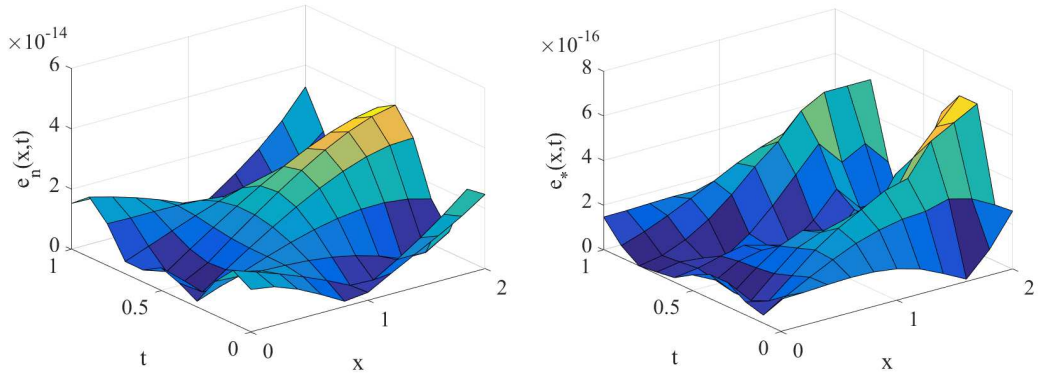

(a) (b)

FIGURE 6 When $n = 4$, the absolute and correction errors between the numerical solution and the exact solution of the equation solved by SCPs method are compared: (a) Absolute error $e_n(x,t)$; (b) Correction error $e^*(x,t)$.

Based on the Section 5, the correction error between the corrected solution and the exact solution can be obtained. **Fig. 6** shows the correction error is smaller than the absolute error between the numerical solution and the exact solution. That is, the correction solution is closer to the exact solution. When the number of terms of the SCPs $n = 4$, the error precision can be improved from 10^{-14} to 10^{-16}. The proposed correction solution improves the accuracy of the algorithm.

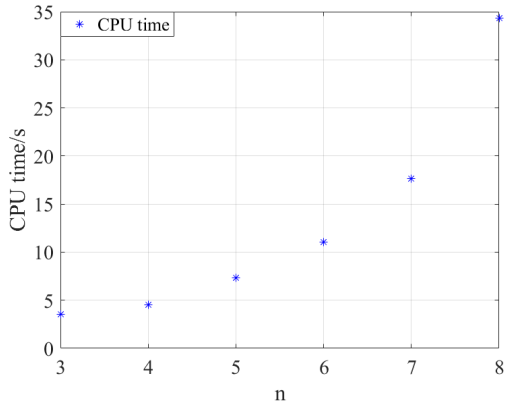

FIGURE 7 The CPU time of the numerical solution of the equation is obtained by the SCPs method when n takes a different number.

The calculate time with different number of terms of the SCPs is shown in **Fig. 7**. An i5-8250U processor with the ram of 8GB has been used to effectuate these calculates. **Fig 7** shows that the calculate time increase with the increase of the number of terms of SCPs. Therefore, the numerical solution can be efficiently approximated in a relatively short time. The proposed numerical algorithm shows excellent calculating efficiency and could solve the fractional partial differential equations quickly.

6.2 Numerical solution of the deformation of visco-elastic beam

The material parameters in FDE model for two visco-elastic polymeric materials (HDPE and PEEK) are defined in **Table 2** and **3** [5]:

TABLE 2 The simulation parameters of HDPE and PEEK in FDE constitutive model.

Material	$\rho\,(\mathrm{kg}/m^3)$	α	η
HDPE	960	0.1603	3.341×10^5
PEEK	1290	0.2341	5.50×10^6

TABLE 3 The simulation parameters of HDPE in FDKV constitutive model.

Material	β	γ	η_1	η_2
HDPE	0.3320	0.1088	2.874×10^5	1.558×10^5

The length of the beam is $l = 5$ m and its cross-section area is $A = 0.04\ \mathrm{m}^2$. The moment of inertia of the beam is $I = \frac{(0.2)^4}{12}\ \mathrm{m}^4$.

The beam is fixed at both ends, so the boundary conditions are as follows:

$$\omega(x,t) = 0,\ \frac{\partial\omega(x,t)}{\partial x} = 0,\ x = 0, l \tag{57}$$

The initial conditions of the system are:

$$\omega(x,0) = 0,\ \frac{\partial\omega(x,t)}{\partial t} = 0 \tag{58}$$

6.2.1 HDPE beam with FDKV model

In this section, the governing equation with FDKV model was used to describe the visco-elastic behavior of the HDPE beam. The deflections, strain and stress of HDPE beam are obtained by using the proposed SCPs algorithm. The deflections of the beam under different load conditions (Heaviside in cases (a) and (b), harmonics in case (c) and linear values in case (d)) are shown in **Fig. 8**.

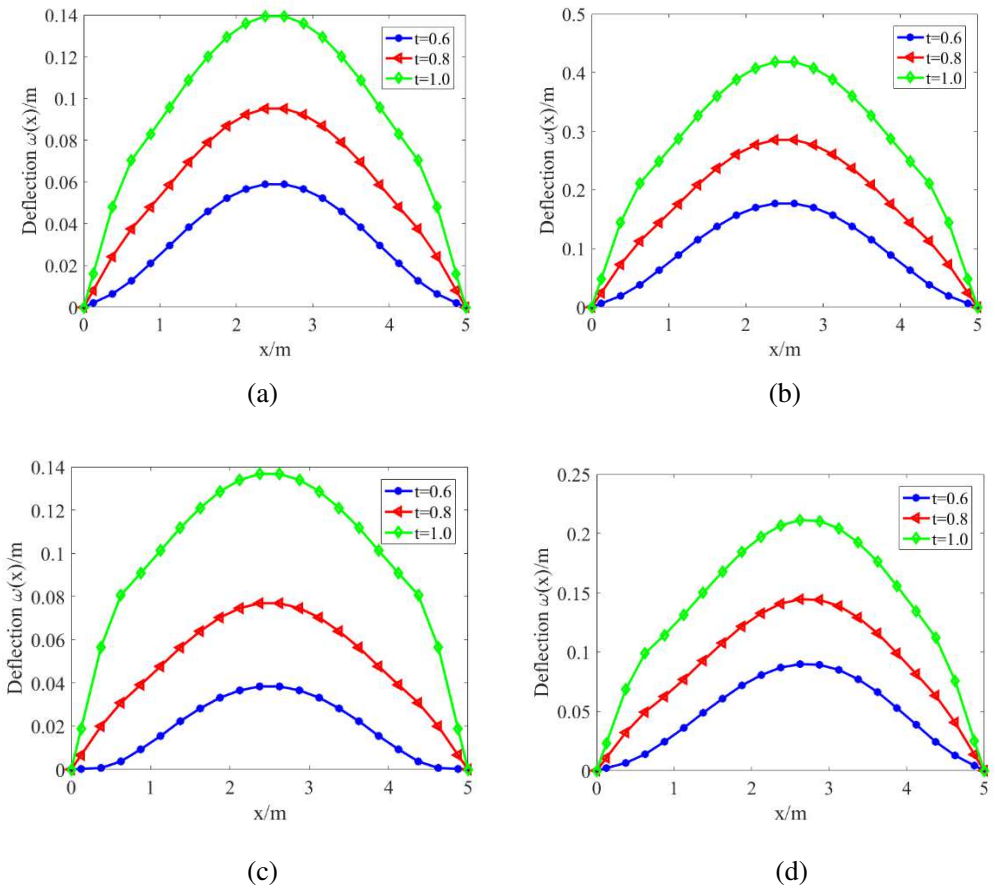

FIGURE 8 Numerical solutions of deflection of the HDPE beam under different load conditions: (a) $f(x,t) = 10Heaviside(t)$; (b) $f(x,t) = 30Heaviside(t)$; (c) $f(x,t) = 10\pi \sin t$; (d) $f(x,t) = 10 + 2x$.

The beam deflection curves in function of x at different loading time are shown in **Fig. 8**. The deflection of the beam increases with x and arrives the maximum value at $x = 2.5$ m. The displacement of the beam is symmetric with respect to the axis $x = 2.5$ m. The deflection curves

of the beam at different loading time are shown in **Fig. 8**. These curves follow the same tendency under the different load conditions. The deflection of the beam increases with the applied load according to the comparison between the case (a) and (b). The similar results have been observed in case (c) and (d), the displacement of the beam increases with the loading time and the most important value of the deflection is obtained in the middle of the beam. In reference [36], the mechanical properties of Euler Bernoulli beams are described by integral order control equations. The simulated displacement images of beams are shown in Figures 4 and 5 in the reference. The trend of the image is consistent with that of the displacement image. Compared with the reference [36], the validity and accuracy of the proposed algorithm are further verified.

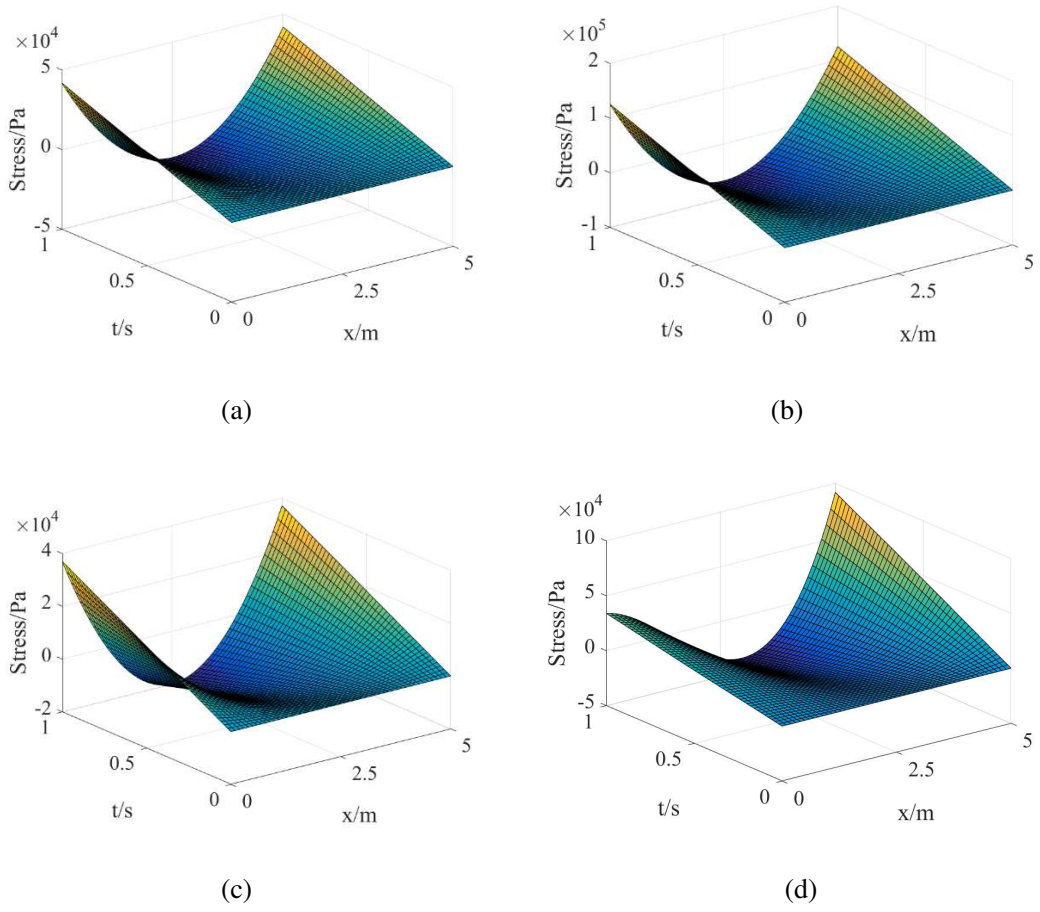

FIGURE 9 The stress of HDPE beams under different external loads: (a) $f(x,t) = 10Heaviside(t)$; (b) $f(x,t) = 30Heaviside(t)$; (c)$f(x,t) = 10\pi \sin t$; (d) $f(x,t) = 10 + 2x$.

Based on Eq. (18), the stress of the beam under different load conditions (Heaviside, harmonics and linear loads) is illustrated in **Fig. 9**. The stress increases with the loading time for all kinds of load conditions. At the same loading time, the value of the stress is minimum when near $x = 2.5$ m, and the force resisting external load is the weakest, and the displacement is the smallest. The value of the stress increase when the position is close to the fixed end of the beam, and the greater the force against external load, the smaller the displacement. The deformation of the beam is symmetric with respect to the axis $x = 2.5$ m, which is similar with the observation in

the deflection. It can be seen that the values of deflection and stress are successfully obtained by using the proposed numerical algorithm. The numerical results are consistent with the experimental investigations of the beam vibration deformation [37,38].

6.2.2 Comparison of HDPE and PEEK beams

In this section, the governing equation with FDE model was used to describe the visco-elastic behavior of the HDPE and PEEK beam. The material parameters of the polymers in the FDE model were put into the Eq. (23), which is solved by using the proposed numerical algorithm. The deflection of the HDPE and PEEK beam in function of x under different load conditions is shown in **Fig. 10**.

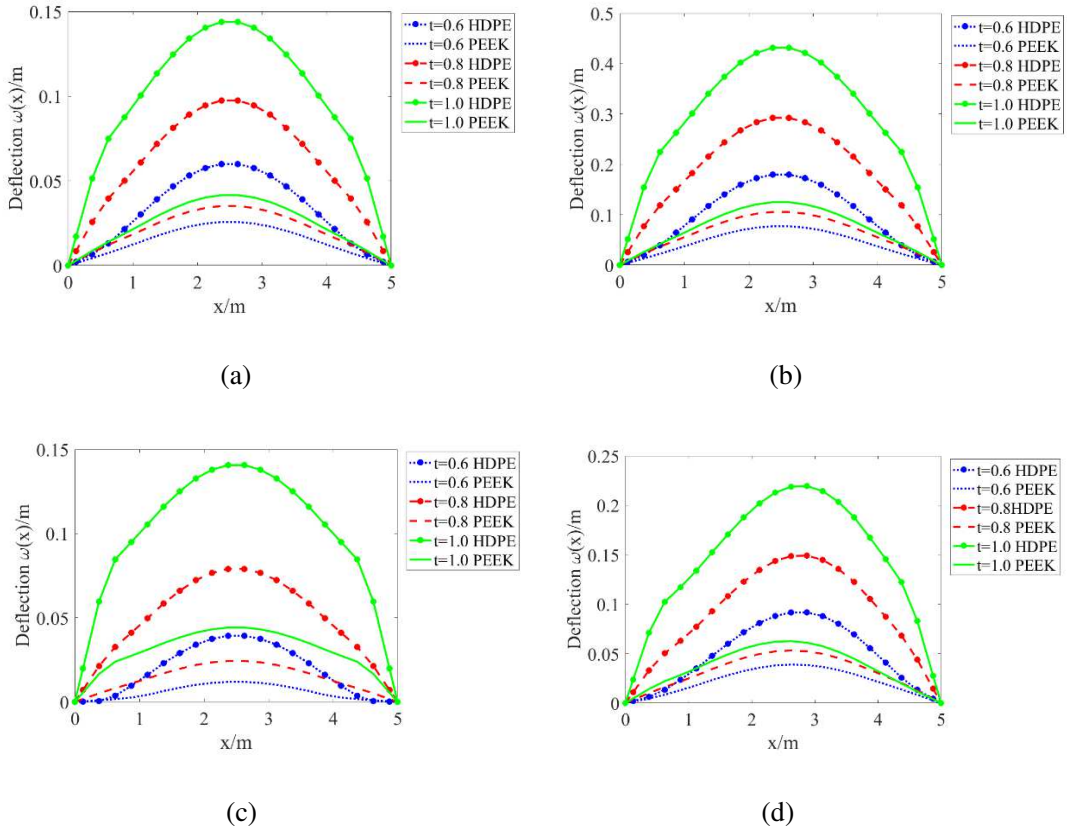

FIGURE 10 Comparison of the deflection of the HDPE and PEEK beams under different load conditions: (a) $f(x,t) = 10Heaviside(t)$; (b) $f(x,t) = 30Heaviside(t)$; (c) $f(x,t) = 10\pi \sin t$; (d) $f(x,t) = 10 + 2x$.

Based on **Fig. 10**, the deflection of the PEEK beam is less than that of the HDPE beam under the same load condition. The difference of the deflection of these two polymers becomes more important with the loading time. One can conclude that the PEEK exhibits better bending resistance than the HDPE due to its smaller deflection under the same load conditions. This is consistent with the material properties, because the elastic modulus of PEEK is more important than that of HDPE in the same thermal and mechanical conditions. The proposed numerical algorithm seems to be efficient to predict the vibration deformation of the visco-elastic polymers under various load conditions.

6.2.3 Comparison of FDE and FDKV models

In this section, the governing equations with FDE and FDKV model were used to describe the visco-elastic behavior of the HDPE beam. The objective of this work is to investigate the sensibility of the visco-elastic models in the prediction of beam deflection under different load conditions. The deflection of the HDPE beam, which is calculated by the governing equation based on FDE model and FDKV model is shown in **Fig. 11**.

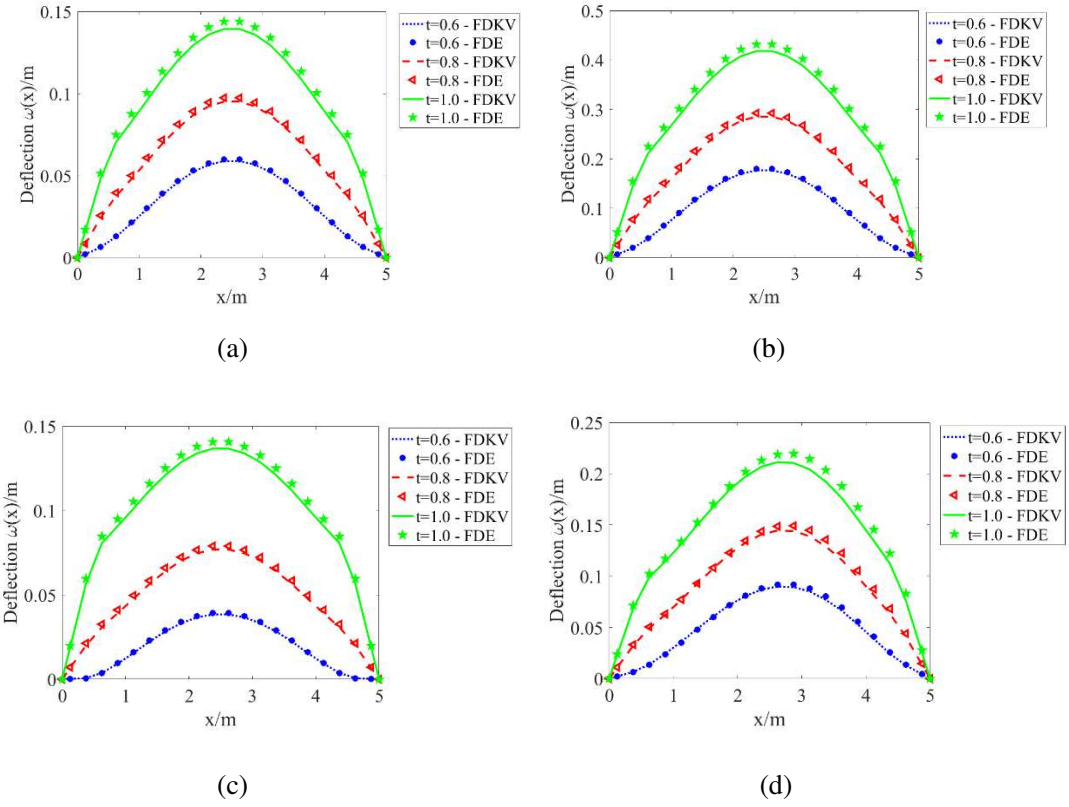

FIGURE 11 Comparison of the deflection of the HDPE beam with FE and FDKV models under different load conditions: (a) $f(x,t) = 10Heaviside(t)$; (b) $f(x,t) = 30Heaviside(t)$; (c) $f(x,t) = 10\pi \sin t$; (d) $f(x,t) = 10 + 2x$.

Based on **Fig. 11**, the deflection of the HDPE beam with the FDE model is slightly more important than that with the FDKV model under the same load, especially in the positions far from the fixed ends. But the difference between the values of defection with these two models is quite small relative to the length of the beam. One can conclude that the displacements of the beam calculated by using the governing equations with FDE and FDKV models are approximately coincide under the same load, which confirms the efficiency and accuracy of the proposed SCPs method in the numerical solution of the fractional partial differential equations.

7. Conclusion

In this paper, the governing equations of visco-elastic Euler-Bernoulli beams have been created by using the fractional rheological constitutive models. An effective numerical algorithm for solving the governing equations is proposed in the time-domain. The fractional rheological model containing the fractional derivatives is used to analyze the inherent laws of the dynamic performance of visco-elastic damping materials, which can provide a theoretical basis for the research, development and performance prediction of vibration damping materials. Based on the visco-elasticity of the FDE and FDKV constitutive models, the SCPs operator matrix is deduced

and the numerical solution of the governing equations of the visco-elastic beam under different loads is obtained. The displacement solutions of the HDPE beam based on two constitutive models are compared. Different visco-elastic beams have been studied to verify the calculation accuracy and efficiency of the algorithm.

1) Two governing equations based on the FDE and FDKV models are established to analyze the deformation of the visco-elastic Euler-Bernoulli beam. The stress and strain of the beam are obtained by using the proposed algorithm.
2) The proposed method has been validated by the numerical solution of the governing equation. Based on the comparison of the numerical solutions with the FDKV and FDE model, the deflections of the beam are almost completely coincident at different loading time, which permits to verify the accuracy of the algorithm.
3) The displacement solutions of the visco-elastic beam of HDPE and PEEK under uniform load, harmonic load and linear load are compared to investigate the material sensibility of the proposed algorithm. The conclusion is that the displacement of PEEK beam is smaller than that of HDPE beam, when the beam is under the same load condition. The greater the damping of the corresponding visco-elastic material and the better the bending resistance.

ACKNOWLEDGEMENT

This work is supported by the Natural Science Foundation of Hebei Province (A2017203100) in China and Le Studium research professorship award of Centre-Val de Loire region in France.

References

[1] D'more A, Pompo A, Nicolais L. Viscoelastic effects in poly (ether ether ketone) (PEEK) and PEEK-based composites[J]. Composites Science and Technology.1991;41(3):303-325.

[2] Elleuch R, Taktak W. Viscoelastic behavior of HDPE polymer using tensile and compressive loading[J]. Journal of Materials Engineering and Performance. 2006;15(1):111-116.

[3] Lai J, Bakker A. Analysis of the non-linear creep of high-density polyethylene[J]. Polymer. 1995;36(1):93-99.

[4] Guo YL, Bradshaw RD. Isothermal physical aging characterization of Polyether-ether-ketone (PEEK) and Polyphenylene sulfide (PPS) films by creep and stress relaxation[J]. Mechanics of Time-Dependent Materials. 2007;11(1):61-89.

[5] Xu HY, Jiang XY. Creep constitutive models for viscoelastic materials based on fractional derivatives[J]. Computers and mathematics with Applications. 2017;73(6):1377-1384.

[6] Gemant A. On fractional differences[J]. Phil Mag. 1938;25(1):92-96.

[7] Bagley RL, Torvik PJ. On the fractional calculus model of viscoelasticity behavior[J]. Journal of Rheology. 1986;30(1):133-155.

[8] Leung AYT, Yang HX, Zhu P, et al. Steady state response of fractionally damped nonlinear viscoelastic arches by residue harmonic homotopy[J]. Computers and Structures. 2013;121(5):10-21.

[9] Lewandowski R, Pawlak Z. Dynamic analysis of frames with viscoelastic dampers modelled by rheological models with fractional derivatives[J]. Journal of Sound and Vibration. 2011;330(5):923-936.

[10] Kang JH, Zhou FB, Liu C, Liu YK. A fractional non-linear creep model for coal considering

damage effect and experimental validation[J]. International Journal of Non-Linear Mechanics. 2015;76:20-28.
[11] Gioacchino A, Mario DP, Giuseppe F. On the dynamics of non-local fractional viscoelastic beams under stochastic agencies[J]. Composites Part B: Engineering. 2018;137:102-110.
[12] Lewandowski R, Wielentejczyk P. Nonlinear vibration of viscoelastic beams described using fractional order derivatives[J]. Journal of Sound and Vibration. 2017;399:228-243.
[13] Lewandowski R, Baum M. Dynamic characteristics of multilayered beams with viscoelastic layers described by the fractional Zener model[J]. Archive of Applied Mechanics. 2015;85(12):1793-1814.
[14] Fernando C, María JE. Finite element formulations for transient dynamic analysis in structural systems with viscoelastic treatments containing fractional derivative models[J]. International Journal for Numerical Methods in Engineering. 2007;69(10):2173-2195.
[15] Bahraini SMS, Eghtesad M, Farid M, Ghavanloo E. Large deflection of viscoelastic beams using fractional derivative model[J]. Journal of Mechanical Science and Technology. 2013;27(4):1063-1070.
[16] Di PM, Heuer R, Pirrotta A. Fractional visco-elastic Euler–Bernoulli beam[J]. International Journal of Solids and Structures. 2013;50(22-23):3505-3510.
[17] He XQ, Rafiee M, Mareishi S, Liew KM. Large amplitude vibration of fractionally damped viscoelastic CNTs/fiber/polymer multiscale composite beams[J]. Composite Structures. 2015;131: 1111-1123.
[18] Chang JR, Lin WJ, Huang CJ, Choi ST. Vibration and stability of an axially moving Rayleigh beam[J]. Applied Mathematical Modelling. 2010;34(6):1482-1497.
[19] Friswell MI, Adhikari S, Lei Y. Vibration analysis of beams with non-local foundations using the finite element method[J]. International Journal for Numerical Methods in Engineering. 2007;71(11):1365-1386.
[20] Demir DD, Bildik N, Sınır BG. Linear dynamical analysis of fractionally damped beams and rods[J]. Journal of Engineering Mathematics. 2014;85(1):131-147.
[21] Permoon MR, Rashidinia J, Parsa A, Haddadpour H, Salehi R. Application of radial basis functions and sinc method for solving the forced vibration of fractional viscoelastic beam[J]. Journal of Mechanical Science and Technology. 2016;30(7):3001-3008.
[22] Martinez-Agirre M, Elejabarrieta MJ. Higher order eigensensitivities-based numerical method for the harmonic analysis of viscoelastically damped structures[J]. International Journal for Numerical Methods in Engineering. 2011;88(12):1280-1296.
[23] Martin O. A modified variational iteration method for the analysis of viscoelastic beams[J]. Applied Mathematical Modelling. 2016;40(17):7988-7995.
[24] Meng ZJ, Yi MX, Hang J, Song L. Numerical solutions of nonlinear fractional differential equations by alternative Legendre polynomials[J]. Applied Mathematics and Computation. 2018;336:454-464.
[25] Chen YM, Sun YN, Liu LQ. Numerical solution of fractional partial differential equations with variable coefficients using generalized fractional-order Legendre functions[J]. Applied Mathematics and Computation. 2014;244(2):847-858.
[26] Xie JQ, Yao ZB, Gui HL, Zhao FQ, Liu DY. A two-dimensional Chebyshev wavelets approach for solving the Fokker-Planck equations of time and space fractional derivatives type with variable coefficients[J]. Applied Mathematics and Computation. 2018;332:197-208.

[27] Chen YM, Lu LX, Fu XH. Numerical solution of nonlinear fractional integral differential equations by using the second kind Chebyshev wavelets[J]. Computer Modeling in Engineering and Sciences. 2013;90(5):359-378.
[28] Wang J, Xu TZ, Wei YQ, Xie JQ. Numerical solutions for systems of fractional order differential equations with Bernoulli wavelets[J]. International Journal of Computer Mathematics. 2019;96(2):317-336.
[29] Chen YM, Liu LQ, Liu DY, Boutat D. Numerical study of a class of variable order nonlinear fractional differential equation in terms of Bernstein polynomials[J]. Ain Shams Engineering Journal. 2016;9(4):1235-1241.
[30] Chen YM, Liu LQ, Li BF, Sun YN. Numerical solution for the variable order linear cable equation with Bernstein polynomials[J]. Applied Mathematics and Computation.2014;238(7):329-341.
[31] Fernanda SP, Miguel P, Higinio R. Extrapolating for attaining high precision solutions for fractional partial differential equations[J]. Fractional Calculus and Applied Analysis. 2018;21(6):1506-1523.
[32] Lin YM, Xu CJ. Finite difference/spectral approximations for the time-fractional diffusion equation[J]. Journal of Computational Physics. 2007;225(2):1533-1552.
[33] Taghvafard H, Erjaee GH. Phase and anti-phase synchronization of fractional order chaotic systems via active control[J]. Communications in Nonlinear Science and Numerical Simulation. 2011;16(10):4079-4088.
[34] Wilhelm F. Viscoelasticity [M]. New York: Springer-Verlag Berlin Heidelberg GmbH, 1975.
[35] Du M, Wang Z, Hu H. Measuring memory with the order of fractional derivative[J]. Scientific Reports. 2013;3(7478):3431.
[36] Brito WK.F, Maia CD, Mendonca AV. Bending analysis of elastically connected Euler-Bernoulli double-beam system using the direct boundary element method[J]. Applied Mathematical Modelling. 2019;74:387-408.
[37] Martin O. Stability approach to the fractional variational iteration method used for the dynamic analysis of viscoelastic beams[J]. Journal of Computational and Applied Mathematics. 2019;346(15):261-276.
[38] Yu CX, Zhang J, Chen YM, Feng YJ, Yang AM. A numerical method for solving fractional-order viscoelastic Euler-Bernoulli beams[J]. Chaos, Solitons and Fractals. 2019;128:275-279.

TABLE 4 Nomenclature

Symbol	Explanation
PEEK	Poly (ether ether ketone)

HDPE	High density polyethylene
SCPs	Shifted Chebyshev polynomials
FDE model	Fractional derivative element model
FDKV model	Fractional derivative Kelvin-Voigt model
$\alpha, \beta, \gamma, p_\kappa, q_\kappa$	Fractional derivative order
σ	Normal stress on the cross section
ε	Strain
η, η_1, η_2	Material constants in FDE and FDKV models
${}^{C}D^{\alpha}$, ${}^{C}D^{\beta}$, ${}^{C}D^{\gamma}$	Fractional order differential operator
$\Phi_n(x), \Phi_n(t)$	Family of shifted Chebyshev polynomials
$F_i(x), G_i(x), G_k(x), G_j(x), G_j(t)$	Shifted Chebyshev polynomials
A_n, A_X, A_T, U	Coefficient matrix
P_x^1, P_t^1	First order differential operator matrix
P_t^α	Fractional order differential operator matrix
$Z_n(x)$	Family of basical polynomials
μ_κ, η_κ	Material constants in one-dimensional visco-elastic model
a, y, m, H, T, κ	Non-negative real number
c	Real number on the interval $[-1, 1]$
b	Width of a rectangular cross section
h	Height of a rectangular cross section
x	Position
t	Time
$f(x,t)$	Load
l	Length of beam
A	Cross-sectional area
I	Moment of inertia
ρ	Density of material
$M(x,t)$	Beam bending moment
$L[*]$	Operator for error correction
$R_n(x,t)$	Residual function
$E(x,t)$	Correction error function
$\omega(x,t)$	Exact solution of displacement
$\omega_n(x,t)$	Numerical solution of displacement
$\omega^*(x,t)$	Correction solution of displacement
R_M	Taylor series remainder
$\omega_{T,M}(x,t)$	M^{th} Taylor series expansion of $\omega(x,t)$
$e_n(x,t)$	Absolute error function
$e^*(x,t)$	Correction error function
$\hat{e}(x,t)$	Relative error function